Dynamics of hybrid junctions of Majorana wires

Nilanjan Bondyopadhaya[1] and Dibyendu Roy[2]
[1]*Integrated Science Education and Research Center, Visva-Bharati University, Santiniketan, West Bengal 731235, India*
[2]*Raman Research Institute, Bangalore 560080, India*

(Received 7 January 2019; revised manuscript received 3 May 2019; published 28 June 2019)

We investigate the dynamics of hybrid junctions made of the topological superconductor (TS) and normal metal (N) wires. We consider an X-Y-Z configuration for the junctions where X, Y, Z = TS, N. We assume the wires X and Z are semi-infinite and in thermal equilibrium. We connect the wires X and Z through the short Y wire at some time and numerically study time evolution of the full device. For TS-N-TS devices, we find a persistent, oscillating electrical current at both junctions even in the absence of any phase, voltage, or thermal bias. The amplitude and period of the oscillating current depend on the initial conditions of the middle N wire indicating the absence of thermalization. This zero-bias current vanishes at long times for any of X and Z being an N wire or a TS wire near a topological phase transition. Using properties of different bound states within the superconducting gap, we develop a clear understanding of the oscillating currents.

DOI: 10.1103/PhysRevB.99.214514

I. INTRODUCTION

Recent progress in search of Majorana zero modes (MZMs) in condensed matter systems has generated massive interest for better understanding, control, and engineering of such systems featuring these exotic quasiparticles [1–4]. The MZMs have been theoretically proposed to emerge at the edges of a topological superconductor (TS) wire and to exhibit non-Abelian particle statistics [5–7]. Several experiments have observed significant evidence of MZMs in electrical transport measurements with engineered TS wires [8–12]. These TS wires hosting Majorana quasiparticles are expected to be an essential component of future quantum devices such as fault-tolerant quantum computers. Therefore, it is necessary to investigate various properties including thermalization, transport, and braiding operations in hybrid junctions of TS and normal metal (N) wires.

In the past ten years, there have been many theoretical studies for electrical transport in different junctions of TS and N wires [2,3]. Most of these studies discuss steady-state transport to derive zero-bias conductance [13–17], current-voltage characteristics [16,18], current-phase relation for fractional Josephson effect [18–23], and robust Majorana conductance peaks [24,25]. There are also some time-evolution studies after a quantum quench [26–29] such as when an N wire is suddenly connected to a TS wire. Interestingly, a systematic study for the dynamics of tunneling current in these hybrid devices is missing. In this paper, we study transient and steady-state quantum transport in hybrid junctions of X-Y-Z configuration where X, Y, Z = TS, N (see the cartoon in Fig. 1). We primarily address route to equilibration in these junctions by investigating the dynamics of tunneling current. Ideally, we consider the wires X and Z to be semi-infinite and in thermal equilibrium. However, we can only investigate $L_{X,Z}/L_Y \gg 1$ in our numerics for time evolution where $L_{X,Z}$ and L_Y are the lengths of the wires X or Z and Y, respectively. We connect the wires X and Z through the middle Y wire at some time t_0 and explore time evolution of the full system for various initialization of the middle wire. We probe electrical current through the X-Y and Y-Z junctions at every stage of time evolution. Here we do not consider a voltage bias for a TS-N-TS device which can be incorporated through time-dependent phases in the tunnel couplings across the junctions [18]. In the main part of the paper, we also ignore any effect which can arise due to phase difference of superconducting pairing potential across the junctions of TS wires; therefore, we set the phase of the TS wires to be same (or zero for simplicity) everywhere.

We find a nondecaying, oscillating electrical current at both junctions of a TS-N-TS device even in the absence of any thermal or voltage bias and for identical TS wires (no phase difference). The amplitude and period of the oscillating current depend on the energy eigenstates of the wires which are localized around the junctions and within the superconducting gap of the TS wires, and on the initial conditions of the N wire. Since the wave functions of the energy eigenstates of the N wire in the superconducting gap decay exponentially deep inside the TS wire, they act as bound states. The presence of such bound states prevent equilibration (thermalization) of the middle N wire with the boundary wires [30], and this results into the nonuniqueness (initial-condition dependence) of the persistent current. There is no zero-bias oscillating current at long times in an N-TS-N and an X-N-Z device when any of the X and Z being an N wire or a TS wire near a topological phase transition. In these latter cases, the energy spectrum of one of the boundary wires is gapless. Thus, there is no more bound state from the middle N wire, and the middle wire gets equilibrated with the boundary wire(s). Using properties of different bound states within the superconducting gap in our devices, we develop a theory to reproduce the simulated oscillating current with little numerics.

The details of our study are provided in the following sections and appendices. In Sec. II, we model the TS wires as a one-dimensional (1D) $p-$ wave superconductor of spinless

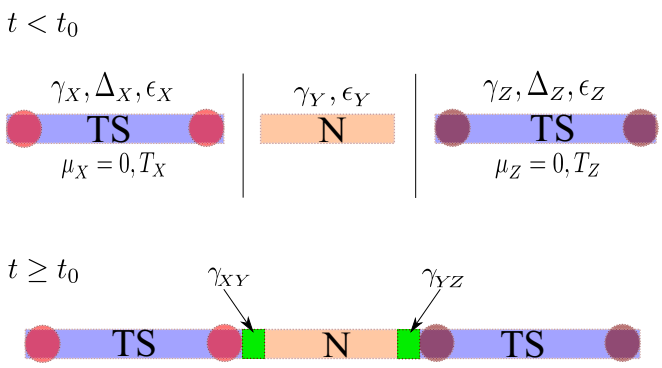

FIG. 1. Schematic of a hybrid device of X-Y-Z configuration where X, Z are made of topological superconductors (TS) and Y is a normal metal (N). It shows the individual components of the device before (top) and after (bottom) their coupling via the tunneling rate γ_{XY} and γ_{YZ}. The red dots indicate Majorana bound states appearing at the edges of the TS wires.

fermions proposed by Kitaev, and we discuss our method here to study the dynamics of such hybrid devices. We present results of the time-evolution study for different hybrid devices made of Kitaev chains in Sec. III. We show in Sec. IV that the main conclusions obtained for Kitaev chains also survive for a more realistic model of TS wires made of spin-orbit coupled semiconductor-superconductor heterostructure in the presence of magnetic field. In Sec. V, we carry out a numerically inexpensive study of the time evolution of density matrix by solely keeping the contribution of the spatially localized bound states. We discuss related recent studies and the possibility of an experimental test of our findings in Sec. VI. We include four appendices: Appendix A and Appendix C to present the temporal evolution of currents in an N-TS-N device and a TS-N-N device, respectively; Appendix B to show the change in the temporal evolution of currents in a TS-N-TS device for a longer length of N wire and a phase difference between the TS wires; and Appendix D to clarify the role of tunnel coupling.

II. MODEL AND METHOD

We now introduce the Hamiltonian for various components of the hybrid junctions. We model the N wire as a noninteracting tight-binding chain of spinless fermions and the TS wire by the Kitaev chain of a spinless p-wave superconductor [5] everywhere except in Sec. IV where we extend our study to an experimentally realizable model of TS wires [6–9]. We write below a general Hamiltonian H_α which can be used to represent N and TS wires by tuning the parameters,

$$H_\alpha = -\gamma_\alpha \sum_{l'=1}^{L_\alpha - 1} (c_{l'}^\dagger c_{l'+1} + c_{l'+1}^\dagger c_{l'}) - \epsilon_\alpha \sum_{l'=1}^{L_\alpha} c_{l'}^\dagger c_{l'} + \Delta_\alpha \sum_{l'=1}^{L_\alpha - 1} (c_{l'}^\dagger c_{l'+1}^\dagger + c_{l'+1} c_{l'}), \quad (1)$$

where $c_{l'}$ ($c_{l'}^\dagger$) indicates annihilation (creation) operator of a spinless fermion at site l' of the wire segment $\alpha = \mathrm{X,Y,Z}$. Here, the parameters $\gamma_\alpha, \epsilon_\alpha$, and Δ_α denote, respectively, hopping, on-site energy, and superconducting pairing energy, and we take them to be real. The Hamiltonian H_α indicates an N wire in the absence of pairing ($\Delta_\alpha = 0$). In the presence of pairing $\Delta_\alpha \neq 0$, the superconducting wire undergoes a topological phase transition as ϵ_α is increased across $2\gamma_\alpha$. The wire is in a topological phase for $|\epsilon_\alpha| < 2|\gamma_\alpha|$ and the TS wire hosts two MZMs at the opposite ends of the wire for a relatively long wire. The wire is in a topologically trivial phase without the MZMs for $|\epsilon_\alpha| > 2|\gamma_\alpha|$. The topological phase transition near $|\epsilon_\alpha| = 2|\gamma_\alpha|$ is also accompanied by a bulk-gap closing. The superconducting wire has a large bulk gap in its spectrum both in the topologically nontrivial and trivial phases, and the gap vanishes at the topological phase transition around $|\epsilon_\alpha| = 2|\gamma_\alpha|$.

The tunneling Hamiltonian for the X-Y and Y-Z junction is independent of nature of X, Y, Z, and we take it of the following form:

$$H_{\alpha\beta} = -\gamma_{\alpha\beta}(c_{l'}^\dagger c_{l'+1} + c_{l'+1}^\dagger c_{l'}), \quad (2)$$

where $\alpha\beta = \mathrm{XY}$, $l' = L_\mathrm{X}$, and $\alpha\beta = \mathrm{YZ}$, $l' = L_\mathrm{X} + L_\mathrm{Y}$, respectively, for the X-Y and Y-Z junctions. For simplicity, we assume here the tunneling rate $\gamma_{\alpha\beta}$ (with $\gamma_{\alpha\beta} \ll \gamma_\alpha, \gamma_\beta$) to be the same for both junctions, i.e., $\gamma_{\mathrm{XY}} = \gamma_{\mathrm{YZ}} = \gamma'$. The full Hamiltonian of the hybrid device is $H_\mathrm{F} = H_\mathrm{X} + H_\mathrm{Y} + H_\mathrm{Z} + H_{\mathrm{XY}} + H_{\mathrm{YZ}}$. The full device consists of $L = L_\mathrm{X} + L_\mathrm{Y} + L_\mathrm{Z}$ number of fermionic sites. Using conservation of electrical charges across the junctions, we define the electrical current at the junctions as

$$J_{\alpha\beta} = i\gamma_{\alpha\beta}\langle (c_{l'}^\dagger c_{l'+1} - c_{l'+1}^\dagger c_{l'})\rangle, \quad (3)$$

where again $\alpha\beta = \mathrm{XY}, l' = L_\mathrm{X}$, and $\alpha\beta = \mathrm{YZ}, l' = L_\mathrm{X} + L_\mathrm{Y}$, respectively, for the X-Y and Y-Z junctions. The expectation $\langle .. \rangle$ defines averaging over the initial states of the wires.

Due to the pairing term Δ_α in the superconducting parts of the hybrid device, it is convenient to use a basis $\mathbf{a} \equiv (a_1, a_2, \ldots, a_{2L-1}, a_{2L})^T = (c_1, c_1^\dagger, \ldots, c_L, c_L^\dagger)^T$ to write the quadratic Hamiltonian $H_\mathrm{F} = \frac{1}{2}\mathbf{a}^\dagger \mathcal{H}^\mathrm{F} \mathbf{a} = \frac{1}{2}\sum_{l,m} \mathcal{H}_{lm}^\mathrm{F} a_l^\dagger a_m$ in terms of the matrix $\mathcal{H}_{lm}^\mathrm{F}$ [31,32]. Thus, $a_{2l} = a_{2l-1}^\dagger$. Clearly, the index l in a_l (or $a_l^\dagger$) does not represent the actual physical site of the wire. For a given l, one can define a map to the physical site l' of spinless fermions as $l' = (l+1)/2$ for odd values of l and $l' = (l/2)$ for even values of l. We consider the wires X and Z are in thermal equilibrium at temperatures $T_{\mathrm{X,Z}}$ and chemical potentials $\mu_{\mathrm{X,Z}}$ before we connect them through the middle wire Y at time t_0. For isolated X and Z wires, we have $H_\alpha = \frac{1}{2}\sum_{l,m} \mathcal{H}_{lm}^\alpha a_l^\dagger a_m$ with $l, m = 1, 2, \ldots, 2L_\mathrm{X}$ for $\alpha = \mathrm{X}$, and $l, m = 2(L_\mathrm{X} + L_\mathrm{Y}) + 1, 2(L_\mathrm{X} + L_\mathrm{Y}) + 2, \ldots, 2L$ for $\alpha = \mathrm{Z}$. Therefore, we can write

$$\sum_m \mathcal{H}_{lm}^\alpha \psi_q^\alpha(m) = \lambda_q^\alpha \psi_q^\alpha(l), \quad (4)$$

where $\psi_q^\alpha(m)$ and λ_q^α represent the eigenvectors and eigenvalues of the wire $\alpha = \mathrm{X,Z}$. Thus, the equilibrium density matrix for sites on the isolated boundary wires

$$\langle a_l^\dagger(t_0) a_m(t_0)\rangle = \sum_q \psi_q^{\alpha *}(l)\psi_q^\alpha(m) f\left(\lambda_q^\alpha, \mu_\alpha, T_\alpha\right), \quad (5)$$

with $l, m = 1, 2, \ldots, 2L_X$ for $\alpha = X$ and $l, m = 2(L_X + L_Y) + 1, 2(L_X + L_Y) + 2, \ldots, 2L$ for $\alpha = Z$. Here, $f(\lambda_q^\alpha, \mu_\alpha, T_\alpha) = 1/(e^{(\lambda_q^\alpha - \mu_\alpha)/k_B T_\alpha} + 1)$ is the Fermi function.

We also assume that the operators from different X, Y, Z wires are uncorrelated when they are disconnected at t_0. Therefore, we have

$$\langle a_l^\dagger(t_0) a_m(t_0)\rangle = \langle a_l(t_0) a_m^\dagger(t_0)\rangle = \langle a_l(t_0) a_m(t_0)\rangle = \langle a_l^\dagger(t_0) a_m^\dagger(t_0)\rangle = 0\,, \tag{6}$$

where l and m represent indices corresponding to two different wires of the hybrid device. We here do not take a thermal distribution for the middle wire Y at t_0. Instead, we choose some arbitrary initial density matrix of wire Y, such as

$$\langle a_{2l'}(t_0) a_{2m'-1}(t_0)\rangle = \begin{cases} n_{l'} & \text{when} \quad l' = m' \\ 0 & \text{when} \quad l' \neq m' \end{cases} \tag{7}$$

for physical sites: $l', m' \in \{L_X + 1, \ldots, L_X + L_Y\}$ and $n_{l'}$ denotes the number of fermions at a site l'. We wish to check whether the density matrix of the full device in the long-time limit $t \to \infty$ becomes independent of the initial density matrix of the middle wire. Such independence would indicate thermalization of the Y wire by the X and Z wires. We carry out this job by calculating time evolution of electrical current at the junctions. So, we connect the wires by the tunneling Hamiltonians at time t_0 and study the time evolution of the full device using the Heisenberg equations of motion. The solution of these equations of motion is given by

$$\mathbf{a}(t) = i\mathcal{G}^+(t - t_0)\mathbf{a}(t_0), \tag{8}$$

where $\mathcal{G}^+(\tau) = -ie^{-iH_F\tau}\theta(\tau) = \sum_{l,m} \mathcal{G}^+_{lm}(\tau) a_l^\dagger a_m$ is the retarded Green's function of the full device and the matrix elements are $\mathcal{G}^+_{lm}(\tau) \equiv [-ie^{-i\mathcal{H}^F\tau}]_{lm}\theta(\tau)$. Here, $\theta(\tau)$ is the Heaviside step function. Suppose, $\Psi_q(m)$ and Λ_q denote the eigenvectors and eigenvalues of the full Hamiltonian H_F. Therefore,

$$\sum_{m=1}^{2L} \mathcal{H}^F_{lm}\Psi_q(m) = \Lambda_q\Psi_q(l),\ l = 1, 2, \ldots, 2L. \tag{9}$$

We apply the above relations to write the matrix elements of the full Green's function in the following form for $t > t_0$:

$$\mathcal{G}^+_{rs}(t - t_0) = -i\sum_{q=1}^{2L} \Psi_q(r)\Psi_q^*(s)e^{-i\Lambda_q(t-t_0)}\,, \tag{10}$$

where $r, s \in \{1, \ldots, 2L\}$. Now, we can write the time-evolved density matrix of the full device as

$$\langle a_l^\dagger(t) a_m(t)\rangle = \sum_{r,s=1}^{2L} \mathcal{G}^+_{ms}(t - t_0)\langle a_r^\dagger(t_0) a_s(t_0)\rangle[\mathcal{G}^+_{lr}(t - t_0)]^\dagger, \tag{11}$$

where we plug the initial density matrix $\langle a_r^\dagger(t_0) a_s(t_0)\rangle$ from Eqs. (5)–(7). Using Eqs. (11) and (3), we evaluate the time evolution of the electrical current at the junctions. These are given by

$$J_{XY}(t) = 2\gamma_{XY}\mathrm{Im}\big[\langle a^\dagger_{2L_X+1}(t) a_{2L_X-1}(t)\rangle\big], \tag{12}$$

$$J_{YZ}(t) = 2\gamma_{YZ}\mathrm{Im}\big[\langle a^\dagger_{2(L_X+L_Y)+1}(t) a_{2(L_X+L_Y)-1}(t)\rangle\big]. \tag{13}$$

III. RESULTS FOR KITAEV CHAIN

In the following numerical analysis, we fix $\gamma_X = \gamma_Z = \gamma > \gamma_Y$ so the bands of the boundary wires are broader than that of the middle. An N-N-N device in the above setup has been studied in detail in Ref. [30] and it has been shown that there is a unique nonequilibrium steady state (independent of initial values of $n_{l'}$) in the device when there is no single particle bound state from the middle wire (the band of wire Y lies within that of X and/or Z).

First, we investigate dynamics of an N-TS-N device whose steady-state transport characteristics are extensively studied both theoretically [13–17] as well as experimentally [8,9,12] for detection of MZMs [33]. We here prepare the decoupled N wires of our N-TS-N device initially in thermal equilibrium. We find from our numerics (check Appendix A) that the nonequilibrium steady-state transport in the N-TS-N device seems to be independent of the initial conditions of the finite TS wire when the band of the N wires is wider than that of the TS wire. Our present finding of unique nonequilibrium steady state in the N-TS-N device validates all those previous steady-state transport analyses [16,17] in this system.

Next, we consider a TS-N-TS device which has been investigated for the Josephson effect in topological systems [18–20,22]. We take the temperature of both the TS wires to be the same and very low, and set their chemical potential to zero. Then, one would naively expect zero electrical current in such junctions of identical TS wires at long times. Surprisingly, we find a persistent and oscillating electrical current at both the junctions of the TS-N-TS device. In Fig. 2, we show time evolution of $J_{XY}(t)$ from $t_0 = 0$ for different initial density $n_{l'}$ of the middle N wire. The amplitude and period of the current oscillation in Figs. 2(a) and 2(b) depend on the initial density of the N wire. For example, there is only a single oscillation period in Fig. 2(a) for initial density, $n_1 = n_2 = n_3 = 0$, while there are two oscillation periods (a short time and a long time) in Fig. 2(b) for $n_1 = 0, n_2 = n_3 = 1$. Thus, our TS-N-TS device does not equilibrate.

The absence of a unique long-time steady state (equilibration) in a TS-N-TS device is due to the presence of bound states near the junctions. The wave functions of these bound states decay exponentially deep inside the TS wires. The energy of these bound states lies within the superconducting gap of the TS wires. Apart from the Majorana bound states (MBSs) of the TS wires near the intersections, there can be such bound states originating from the N wire, and they are commonly known as the Andreev bound states. We observe that the amplitude and period of the current oscillation in the TS-N-TS device also depend on the total number of such bound states near the junctions (see Appendix B). For example, there are two midgap states with energy ± 0.12236 at the edges of TS wires near the intersections as well as two energy eigenstates (at energy ± 0.16795) from the middle N wire inside the superconducting

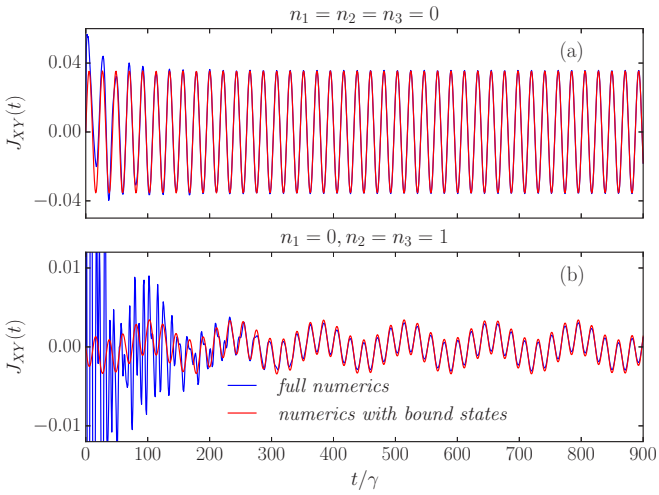

FIG. 2. Temporal evolution of the zero-bias current $J_{XY}(t)$ in a TS-N-TS device made of identical TS wires, and the role of N wire's initial density $n_{l'}$. The blue curves are obtained from full numerics and the red curves are from numerics with only bound states. In all panels, $L_X = L_Z = 900$, $L_Y = 3$, $\gamma_X = \gamma_Z = 1$, $\gamma_Y = 0.5$, $\Delta_X = \Delta_Z = 0.3$, $\epsilon_X = \epsilon_Z = 0$, $\epsilon_Y = 0.05$, $\gamma_{XY} = \gamma_{YZ} = 0.25$, and $T_X = T_Z = 0.02$. The above parameters (except lengths) are in units of γ.

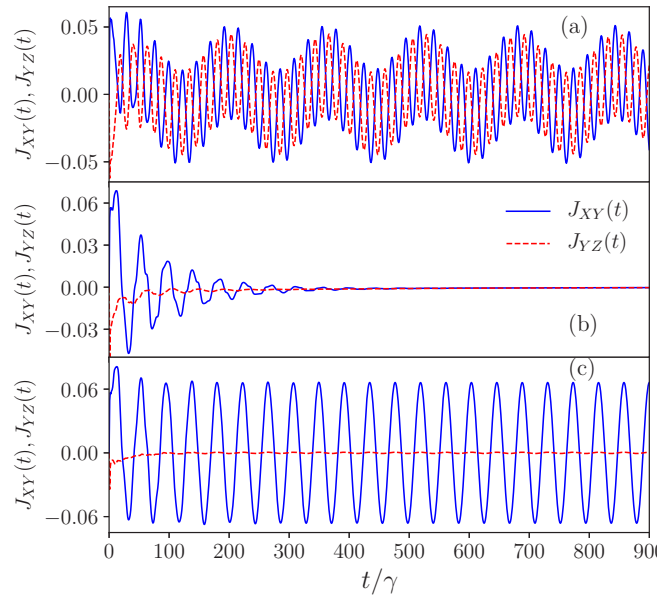

FIG. 3. Nature of zero-bias currents in a TS-N-Z device when the on-site energy of the superconducting Z wire is swept through a topological phase transition. The blue full lines are for $J_{XY}(t)$ and the red dashed lines are for $J_{YZ}(t)$. The on-site energy $\epsilon_Z = 1, 2, 2.5$ in panels (a), (b), and (c), respectively. In all panels, $L_X = L_Z = 900$, $L_Y = 3$, $\gamma_X = \gamma_Z = 1$, $\gamma_Y = 0.5$, $\Delta_X = \Delta_Z = 0.3$, $\epsilon_X = 0$, $\epsilon_Y = 0.05$, $\gamma_{XY} = \gamma_{YZ} = 0.25$, $n_{l'} = 0$, and $T_X = T_Z = 0.02$. The above parameters (except lengths) are in units of γ.

gap for the TS-N-TS device in Fig. 2. The energy of midgap states from the TS wires near the junctions is nonzero due to hybridization of the MBSs of the TS wires through the short middle wire (check Appendix E). From these bound state energies, we derive the periods of short and long time oscillations, respectively, as $2\pi/(0.16795 + 0.12236) \approx 21.6$ and $2\pi/(0.16795 - 0.12236) \approx 137.8$, which are in good agreement with the simulated periods in Fig. 2. In Fig. 8, we further show that the amplitudes of current oscillations remain almost the same as in Fig. 2 when there is no hybridization of the MBSs of the TS wires and the energy of midgap states from the TS wires is almost zero (Appendix E). However, the periods of current oscillations in Fig. 8 are different from Fig. 2 due to the change in energy of the bound states.

To further illustrate the role of these bound states in the absence of equilibration, we study time evolution in a TS-N-Z device where we either apply an N wire for Z or tune the on-site energy of a superconducting Z wire to sweep through a topological phase transition. We do not find any persistent, oscillating electrical current in a TS-N-N device in the absence of bias and we show it in Appendix C. The band of a semi-infinite N wire in our model is continuum without a bulk gap. Therefore, the MBS of the TS wire near the junctions as well as the energy levels of the middle N wire do equilibrate with the boundary N wire; thus there is no oscillating current.

We find persistent, oscillating currents [e.g., check Fig. 3(a)] in a TS-N-Z device in the absence of voltage or thermal bias when $|\epsilon_Z| < 2|\gamma_Z|$, such that there are MBSs at the edges of the topological Z wire, and the bulk gap ($\sim|\epsilon_Z - 2\gamma_Z|$) in the energy spectrum of the Z wire is much larger than γ_{YZ}^2–dissipation induced by the coupling between Y and Z wires. Again, we can separately estimate the periods of oscillating currents in Fig. 3(a) using the bound state energies, and they are $2\pi/(0.15455 + 0.11557) \approx 23.3$ and $2\pi/(0.15455 - 0.11557) \approx 161.2$. Regardless of the initial density of the middle N wire, there is no persistent, oscillating electrical current at the long time in a TS-N-Z device for $|\epsilon_Z| \approx 2|\gamma_Z|$ when there is either no bulk gap in the energy spectrum or a bulk gap which is smaller or the same order of γ_{YZ}^2. In Fig. 3(b), we show rapid decays of $J_{XY}(t)$ and $J_{YZ}(t)$ to zero with time from initial time $t_0 = 0$ when $|\epsilon_Z| = 2|\gamma_Z|$. We also notice in Fig. 3(b) that the amplitude of $J_{YZ}(t)$ is much smaller than $J_{XY}(t)$ in the time duration when they are nonzero. The last fact indicates that such decays of $J_{XY}(t)$ and $J_{YZ}(t)$ are due to equilibration by the thermal Z wire which affects the YZ junction more than the XY junction. Finally, we show oscillating $J_{XY}(t)$ and $J_{YZ}(t)$ in Fig. 3(c) when the Z wire is in a topologically trivial phase with a large bulk gap for $|\epsilon_Z| > 2|\gamma_Z|$. However, the amplitude of $J_{YZ}(t)$ is almost two orders smaller than $J_{XY}(t)$ due to the large bulk gap and the absence of MBS in the Z wire, making the effective coupling between the Y and Z wires much smaller than that between the Y wire and the MBS in the TS wire. The pattern of oscillation in Fig. 3(c) differs from that in Fig. 3(a) due to the presence of an extra MBS in the topological Z wire near the junction in case of Fig. 3(a). The energy of MBS near the junction of the left TS wire remains almost zero due to negligible hybridization when the Z wire is topologically trivial (check Appendix E). The period of current oscillation in Fig. 3(c) is then estimated solely by the bound-state energy from the middle N wire as $2\pi/0.14833 \approx 42.4$.

It is clear from Figs. 2 and 3 that the zero-bias current oscillations of sizable amplitude persist in these hybrid devices

only when there is a midgap state or an MBS at that junction from the adjoining TS wire. Therefore, we can conclude that the large-amplitude zero-bias current oscillation in these systems is a direct signature of midgap bound states (due to hybridized or nonhybridized MBSs) of the superconducting boundary wire(s).

IV. PERSISTENT OSCILLATING CURRENTS IN SEMICONDUCTOR-SUPERCONDUCTOR HETEROSTRUCTURE JUNCTION

In the preceding sections, we have discussed the absence of equilibration and the persistent current oscillations in idealistic TS-N-TS device where these TS wires are 1D p-wave superconductors of spinless fermions proposed by Kitaev. The Kitaev's spinless p-wave chain can be experimentally realized in a 1D semiconductor-superconductor heterostructure which consists of a spin-orbit coupled semiconductor nanowire proximity coupled to an s-wave superconductor, and in the presence of Zeeman spin splitting along the direction of the wire. For a particular value of Zeeman field B above the critical field $B_c(=\sqrt{\Delta^2+\epsilon^2})$, this heterostructure (semiconductor Majorana wire) hosts MBSs at the edges [1,6]. Here, Δ is the s-wave superconducting pairing potential proximity induced in the semiconductor and ϵ is the chemical potential of the semiconductor nanowire. To investigate the fate of persistent oscillating current in an experimentally realizable system, we consider a generalized model of the junction in which the middle Y wire is also a Rasbha spin-orbit-coupled semiconductor (SM) wire with Zeeman interaction. We choose such a junction because it would be convenient to realize in experiments with the TS wires made of semiconductor-superconductor heterostructures [8,9,12]. The full Hamiltonian of such TS-SM-TS device is given by

$$H_{\rm F} = H_{\rm X}^{\rm SS} + H_{\rm Y}^{\rm SM} + H_{\rm Z}^{\rm SS} + H_{\rm XY} + H_{\rm YZ}. \tag{14}$$

The Hamiltonian of the TS wires derived from semiconductor-superconductor heterostructures in the presence of a magnetic field is represented by $H_\alpha^{\rm SS}$:

$$H_\alpha^{\rm SS} = \sum_{l'=I_\alpha}^{N_\alpha-1}\Big[-\gamma_\alpha\sum_{\sigma=\uparrow,\downarrow}(c_{l',\sigma}^\dagger c_{l'+1,\sigma}+c_{l'+1,\sigma}^\dagger c_{l',\sigma})+\zeta_\alpha(c_{l'+1,\uparrow}^\dagger c_{l',\downarrow}-c_{l'+1,\downarrow}^\dagger c_{l',\uparrow}+c_{l',\downarrow}^\dagger c_{l'+1,\uparrow}-c_{l',\uparrow}^\dagger c_{l'+1,\downarrow})\Big]$$
$$+2(\epsilon_\alpha-\gamma_\alpha)\sum_{l'=I_\alpha}^{N_\alpha}\sum_{\sigma=\uparrow,\downarrow}\left(c_{l',\sigma}^\dagger c_{l',\sigma}-\frac{1}{2}\right)+2\sum_{l'=I_\alpha}^{N_\alpha}[B_\alpha(c_{l',\uparrow}^\dagger c_{l',\downarrow}+c_{l',\downarrow}^\dagger c_{l',\uparrow})-\Delta_\alpha(c_{l',\uparrow}^\dagger c_{l',\downarrow}^\dagger+c_{l',\downarrow}c_{l',\uparrow})],$$

where $\alpha = {\rm X}, {\rm Z}$ for X and Z wires, respectively, with $I_{\rm X}=1$, $N_{\rm X}=L_{\rm X}$, and $I_{\rm Z}=L_{\rm X}+L_{\rm Y}+1$, $N_{\rm Z}=L_{\rm X}+L_{\rm Y}+L_{\rm Z}$. Here, $c_{l',\sigma}^\dagger$ denotes the creation operator of a fermion with spin σ at the physical site l'. The parameters ζ_α, B_α, and Δ_α are the strength of Rashba spin-orbit coupling, Zeeman field, and s-wave superconducting pairing potential, respectively. For $B_\alpha > \sqrt{\Delta_\alpha^2+\epsilon_\alpha^2}$, the αth nanowire is in a topological phase and hosts MBSs at the edges. The Hamiltonian of the middle Y wire reads as

$$H_{\rm Y}^{\rm SM} = \sum_{l'=L_{\rm X}+1}^{L_{\rm X}+L_{\rm Y}-1}\Big[-\gamma_Y\sum_{\sigma=\uparrow,\downarrow}(c_{l',\sigma}^\dagger c_{l'+1,\sigma}+c_{l'+1,\sigma}^\dagger c_{l',\sigma})+\zeta_Y(c_{l'+1,\uparrow}^\dagger c_{l',\downarrow}-c_{l'+1,\downarrow}^\dagger c_{l',\uparrow}+c_{l',\downarrow}^\dagger c_{l'+1,\uparrow}-c_{l',\uparrow}^\dagger c_{l'+1,\downarrow})\Big]$$
$$+2\,(\epsilon_{\rm Y}-\gamma_{\rm Y})\sum_{l'=L_{\rm X}+1}^{L_{\rm X}+L_{\rm Y}}\sum_{\sigma=\uparrow,\downarrow}\left(c_{l',\sigma}^\dagger c_{l',\sigma}-\frac{1}{2}\right)+2B_Y\sum_{l'=L_{\rm X}+1}^{L_{\rm X}+L_{\rm Y}}(c_{l',\uparrow}^\dagger c_{l',\downarrow}+c_{l',\downarrow}^\dagger c_{l',\uparrow}), \tag{15}$$

where ζ_Y and B_Y are, respectively, the strength of Rashba spin-orbit coupling and the Zeeman field of the middle wire. In the above two Hamiltonians, γ_α and ϵ_α denote, respectively, the hopping and the chemical potential of the αth wire. We further consider that the tunneling Hamiltonians also include spin-orbit-coupling terms. Thus, the tunneling Hamiltonians for the X-Y and Y-Z junctions are the following:

$$H_{\alpha\beta} = -\gamma_{\alpha\beta}\sum_{\sigma=\uparrow,\downarrow}(c_{l',\sigma}^\dagger c_{l'+1,\sigma}+c_{l'+1,\sigma}^\dagger c_{l',\sigma})+\zeta_{\alpha\beta}(c_{l'+1,\uparrow}^\dagger c_{l',\downarrow}-c_{l'+1,\downarrow}^\dagger c_{l',\uparrow}+c_{l',\downarrow}^\dagger c_{l'+1,\uparrow}-c_{l',\uparrow}^\dagger c_{l'+1,\downarrow}), \tag{16}$$

where $\alpha\beta = {\rm XY}$, $l'=L_{\rm X}$, and $\alpha\beta = {\rm YZ}$, $l'=L_{\rm X}+L_{\rm Y}$, respectively, for the X-Y and Y-Z junction. Similarly, $\zeta_{\alpha\beta}$ represents the strength of Rashba spin-orbit coupling at the tunnel junction. From the definitions of tunneling Hamiltonians, it follows that the current operators can be written as

$$J_{\rm XY}(t) = 2\gamma_{\rm XY}\sum_{\sigma=\uparrow,\downarrow}{\rm Im}\big[\langle c_{L_{\rm X}+1,\sigma}^\dagger(t)\,c_{L_{\rm X},\sigma}(t)\rangle\big]+2\zeta_{\rm XY}\big({\rm Im}\big[\langle c_{L_{\rm X}+1,\downarrow}^\dagger(t)\,c_{L_{\rm X},\uparrow}(t)\rangle\big]-{\rm Im}\big[\langle c_{L_{\rm X}+1,\uparrow}^\dagger(t)\,c_{L_{\rm X},\downarrow}(t)\rangle\big]\big), \tag{17}$$

$$J_{\rm YZ}(t) = 2\gamma_{\rm YZ}\sum_{\sigma=\uparrow,\downarrow}{\rm Im}\big[\langle c_{L_{\rm X}+L_{\rm Y}+1,\sigma}^\dagger(t)\,c_{L_{\rm X}+L_{\rm Y},\sigma}(t)\rangle\big]$$
$$+2\zeta_{\rm YZ}\Big({\rm Im}\big[\langle c_{L_{\rm X}+L_{\rm Y}+1,\downarrow}^\dagger(t)\,c_{L_{\rm X}+L_{\rm Y},\uparrow}(t)\rangle\big]-{\rm Im}\big[\langle c_{L_{\rm X}+L_{\rm Y}+1,\uparrow}^\dagger(t)\,c_{L_{\rm X}+L_{\rm Y},\downarrow}(t)\rangle\big]\Big). \tag{18}$$

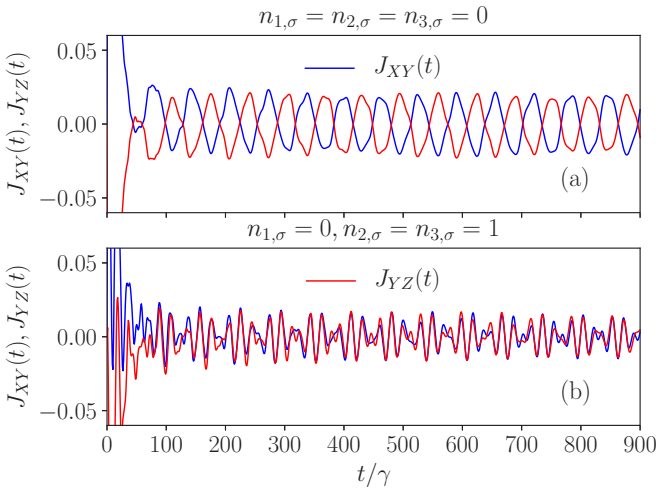

FIG. 4. Temporal evolution of the zero-bias current $J_{\rm XY}(t)$ and $J_{\rm YZ}(t)$ in a TS-SM-TS device made of semiconductor Majorana wires. The initial density $n_{l',\sigma}$ of the middle semiconductor wire is indicated on the heading of the panels. In all panels, $L_{\rm X} = L_{\rm Z} = 900, L_{\rm Y} = 3$, $\gamma_{\rm X} = \gamma_{\rm Z} = \gamma = 1$, $\gamma_{\rm Y} = 0.5$, $\Delta_{\rm X} = \Delta_{\rm Z} = 0.3$, $\epsilon_{\rm X} = \epsilon_{\rm Z} = 0$, $\epsilon_{\rm Y} = 0.05$, $\zeta_{\rm X} = \zeta_{\rm Y} = \zeta_{\rm Z} = 0.2$, $B_{\rm X} = B_{\rm Y} = B_{\rm Z} = 0.4$, $\gamma_{\rm XY} = \gamma_{\rm YZ} = 0.25$, $\zeta_{\rm XY} = \zeta_{\rm YZ} = 0.2$, and $T_{\rm X} = T_{\rm Z} = 0.02$. All above parameters except lengths are in units of γ.

We also generalize the initial density matrix of the boundary wires and the middle wire of the TS-SM-TS device following the previous definitions for the spinless fermions of the TS-N-TS device in Sec. II. Now, $n_{l',\sigma}$ represents the number of fermions with spin σ ($=\uparrow, \downarrow$) at a physical site l' of the middle wire Y initially. We again perform our numerical time evolution from the initial density matrix and evaluate electrical currents at the junctions by using the current operators in Eqs. (17) and (18). As expected, we find the absence of a unique long-time steady state (equilibration) in the TS-SM-TS device (with a realistic model of TS wires) when both the TS wires are in topological phase and there are bound states within the superconducting gap from the middle wire. We also observe initial-condition-dependent persistent current oscillations at both the junctions of aforesaid TS-SM-TS device made of semiconductor Majorana wires. We summarize our findings in Fig. 4.

V. TRUNCATED NUMERICS WITH BOUND STATES

We learn from our discussion in Sec. III for Figs. 2 and 3 that the persistent current oscillation in different hybrid devices in the absence of bias is due to the bound states and their initial preparation. We show below that we can almost reproduce the long-time persistent current oscillations in Figs. 2 and 3 by solely keeping the contributions of the bound states in the current operators in Eqs. (12) and (13). These bound states may be formed inside the middle wire as well as at the edges of the boundary TS wires. To study the contribution of these bound states to the time evolution of density matrix, let us first rewrite the matrix elements of full Green's function $\mathcal{G}^{+}_{rs}(t-t_0)$ in the following way [30]:

$$\begin{aligned}\mathcal{G}^{+}_{rs}(t-t_0) &= \mathcal{G}^{b+}_{rs}(t-t_0) + \mathcal{G}^{c+}_{rs}(t-t_0) \\ &= -i\sum_b \Psi_b(r)\Psi^*_b(s)e^{-i\Lambda_b(t-t_0)} \\ &\quad - i\int d\xi\, \rho^c_{rs}(\xi)e^{-i\xi(t-t_0)}, \end{aligned} \tag{19}$$

where Ψ_b and Λ_b are the full system's eigenvectors and eigenvalues corresponding to the bound states localized around the junctions and the density matrix ρ^c_{rs} is given by a sum over extended (continuum) states Ψ_q of the system, $\rho^c_{rs}(\xi) = \sum^c_q \Psi_q(r)\Psi^*_q(s)\delta(\xi - \Lambda_q)$. Clearly, $\mathcal{G}^{b+}(t-t_0)$ includes all the contributions from the bound states of the full system, while $\mathcal{G}^{c+}(t-t_0)$ incorporates the contribution of the continuum states. If the system does not support bound states, the first term becomes zero and the second term controls the steady-state behavior of the system. However, the scenario changes drastically in the presence of bound states in the system.

Since the bound states are localized, the magnitude of the elements of $\mathcal{G}^{b+}(t-t_0)$ becomes small if we move away from the spatial regions where the bound states are localized. This property of $\mathcal{G}^{b+}(t-t_0)$ is very useful for our computational purpose. Suppose we know that all the bound states are localized within the region $\mathcal{R}_0$. Then it is legitimate to choose the elements of $\mathcal{G}^{b}(t-t_0)$ to be zero outside the region $\mathcal{R}_0$, and we calculate the elements of $\mathcal{G}^{b+}(t-t_0)$ within the region $\mathcal{R}_0$ only. Although the boundary of $\mathcal{R}_0$ is not unique, one can extract the essential features of $\mathcal{G}^{b+}(t-t_0)$ even with a choice of region $\mathcal{R}_0$, which merely encompasses the spatial extent of all the overlapping bound states.

In our numerics for studying persistent current oscillation, we consider a TS-N-TS device where both the boundary TS wires, modeled as the Kitaev chains, have the same chemical potential and temperature. Moreover, we also keep both the superconducting wires in the topologically nontrivial phase away from the topological phase transition. For such a system, there exist two MBSs at the ends of each TS wire. If the TS wires are taken to be sufficiently long, the overlap of the Majorana modes from opposite ends of an individual TS wire becomes almost negligible. However, the overlap between the Majorana modes from the right end of left boundary TS wire and the left end of right boundary TS wire remains finite as long as the length of the middle N wire is not very large. Further, there may also exist bound states within the middle N wire, and it can have nonzero overlap with the Majorana modes localized at the inner edges of the boundary TS wires. In such a situation, essential behavior of the currents in the junctions can be studied with the bound-state-dependent part of the Green's function, i.e., $\mathcal{G}^{b+}(t-t_0)$. As it has been argued already, this $\mathcal{G}^{b+}(t-t_0)$ is chosen to be zero for the region outside $\mathcal{R}_0$ where $\mathcal{R}_0$ is extended from $L_{\rm X} - \delta$ to $L_{\rm X} + L_{\rm Y} + \delta$, where $L_{\rm Y}$ is the length of the N wire, $L_{\rm X}$ is the length of left boundary TS wire, and δ ($\ll L_{\rm X}, L_{\rm Y}, L_{\rm Z}$) is the number of sites inside the boundary wires. The value of δ solely depends on the spatial extent of bound-state wave functions inside the boundary wires. For example, if the wave functions of the bound states around the junctions have

nonzero amplitude up to the L_δ number of sites inside the boundary wires from the junction edge, then $\delta \approx L_\delta$. For our simulation, we find that it is sufficient to choose $\delta \backsim 10$ for the boundary wires with size $L_{\mathrm{X(Z)}} \backsim 10^3$ and the middle wire length $L_{\mathrm{Y}} \backsim 10$.

Given the above discussion, it may be possible to study the time evolution of the bound-state-dependent part of the density matrix using the following expression:

$$\langle a_l^\dagger(t)a_m(t)\rangle_b = \sum_{r,s=2(L_{\mathrm{X}}-\delta)}^{2L_{\mathrm{X}}} \mathcal{G}_{ms}^{b+}(t-t_0)\langle a_r^\dagger(t_0)a_s(t_0)\rangle\left[\mathcal{G}_{lr}^{b+}(t-t_0)\right]^\dagger + \sum_{r,s=2L_{\mathrm{X}}+1}^{2(L_{\mathrm{X}}+L_{\mathrm{Y}})} \mathcal{G}_{ms}^{b+}(t-t_0)\langle a_r^\dagger(t_0)a_s(t_0)\rangle\left[\mathcal{G}_{lr}^{b+}(t-t_0)\right]^\dagger + \sum_{r,s=2(L_{\mathrm{X}}+L_{\mathrm{Y}})+1}^{2(L_{\mathrm{X}}+L_{\mathrm{Y}}+\delta)} \mathcal{G}_{ms}^{b+}(t-t_0)\langle a_r^\dagger(t_0)a_s(t_0)\rangle\left[\mathcal{G}_{lr}^{b+}(t-t_0)\right]^\dagger, \tag{20}$$

where $\langle a_r^\dagger(t_0)a_s(t_0)\rangle$ in the first and third terms denotes the initial equilibrium density matrix of the left and right boundary wires, respectively, and $\langle a_r^\dagger(t_0)a_s(t_0)\rangle$ in the second term represents the initial density matrix of the middle wire. This simplified analytic expression is quite useful in studying the characteristic features of the full density matrix, $\eta_{lm}(t) = \langle a_l^\dagger(t)a_m(t)\rangle$, provided the system hosts bound states with nonzero overlap among themselves. However, if the system does not possess bound states, or the bound states have negligible overlap, the expression in Eq. (20) may fail to depict the actual dynamics of $\eta(t)$ as the continuum part of the full Green's function $[\mathcal{G}^{c+}(t-t_0)]$ starts to play a dominant role. If Eq. (20) fails, then we need to restore to the original expression in Eq. (11) for studying the time evolution, even though it is numerically expensive.

Presence of MBSs at the edges of the boundary TS wires helps us to further simplify the analytical expression for $\langle a_l^\dagger(t)a_m(t)\rangle_b$ in some cases. To this end, let us write the initial equilibrium density matrix of the boundary wires as a summation of two contributions,

$$\begin{aligned}\langle a_r^\dagger(t_0)a_s(t_0)\rangle &= \langle a_r^\dagger(t_0)a_s(t_0)\rangle_{b'} + \langle a_r^\dagger(t_0)a_s(t_0)\rangle_c \\ &= \sum_{b'} \psi_{b'}^{\alpha *}(r)\psi_{b'}^{\alpha}(s) f\left(\lambda_{b'}^{\alpha}, \mu_\alpha, T_\alpha\right) + \sum_{c} \psi_{c}^{\alpha *}(r)\psi_{c}^{\alpha}(s) f\left(\lambda_{c}^{\alpha}, \mu_\alpha, T_\alpha\right),\end{aligned} \tag{21}$$

where ψ_q^α and λ_q^α are the eigenvectors and eigenvalues of the boundary wires $\alpha = \mathrm{X}, \mathrm{Z}$ [see Eq. (4)], and $r, s = 2(L_{\mathrm{X}} - \delta), \ldots, 2L_{\mathrm{X}}$ for $\alpha = \mathrm{X}$, and $r, s = 2(L_{\mathrm{X}} + L_{\mathrm{Y}}) + 1, \ldots, 2(L_{\mathrm{X}} + L_{\mathrm{Y}} + \delta)$ for $\alpha = \mathrm{Z}$. In the second line of Eq. (21), the first term represents the contribution of MBSs localized at the edges of boundary TS wires in the topologically nontrivial phase, and the second term denotes the participation of the continuum states of the boundary wires. Here b' and c subscripts designate the bound states and the continuum states of the boundary TS wires, respectively.

Substituting Eq. (21) in Eq. (20), we get

$$\begin{aligned}\langle a_l^\dagger(t)a_m(t)\rangle_b = &\sum_{r,s=2(L_{\mathrm{X}}-\delta)}^{2L_{\mathrm{X}}} \mathcal{G}_{ms}^{b+}(t-t_0)\langle a_r^\dagger(t_0)a_s(t_0)\rangle_{b'}\left[\mathcal{G}_{lr}^{b+}(t-t_0)\right]^\dagger + \sum_{r,s=2L_{\mathrm{X}}+1}^{2(L_{\mathrm{X}}+L_{\mathrm{Y}})} \mathcal{G}_{ms}^{b+}(t-t_0)\langle a_r^\dagger(t_0)a_s(t_0)\rangle\left[\mathcal{G}_{lr}^{b+}(t-t_0)\right]^\dagger \\ &+ \sum_{r,s=2(L_{\mathrm{X}}+L_{\mathrm{Y}})+1}^{2(L_{\mathrm{X}}+L_{\mathrm{Y}}+\delta)} \mathcal{G}_{ms}^{b+}(t-t_0)\langle a_r^\dagger(t_0)a_s(t_0)\rangle_{b'}\left[\mathcal{G}_{lr}^{b+}(t-t_0)\right]^\dagger + \sum_{r,s=2(L_{\mathrm{X}}-\delta)}^{2L_{\mathrm{X}}} \mathcal{G}_{ms}^{b+}(t-t_0)\langle a_r^\dagger(t_0)a_s(t_0)\rangle_{c}\left[\mathcal{G}_{lr}^{b+}(t-t_0)\right]^\dagger \\ &+ \sum_{r,s=2(L_{\mathrm{X}}+L_{\mathrm{Y}})+1}^{2(L_{\mathrm{X}}+L_{\mathrm{Y}}+\delta)} \mathcal{G}_{ms}^{b+}(t-t_0)\langle a_r^\dagger(t_0)a_s(t_0)\rangle_{c}\left[\mathcal{G}_{lr}^{b+}(t-t_0)\right]^\dagger,\end{aligned} \tag{22}$$

where the initial density matrix in the first and third terms depends on the bound states of the boundary wires, that of the second term relies entirely on the initial conditions at the middle wire, whereas the initial density matrix in the fourth and final term depends on the continuum states of the boundary wires. For the sake of brevity, we can further rewrite Eq. (22) in the following form:

$$\langle a_l^\dagger(t)a_m(t)\rangle_b = \langle a_l^\dagger(t)a_m(t)\rangle_b^B + \langle a_l^\dagger(t)a_m(t)\rangle_b^c, \tag{23}$$

where $\langle a_l^\dagger(t)a_m(t)\rangle_b^B$ represents first three terms on the right-hand side of Eq. (22), and $\langle a_l^\dagger(t)a_m(t)\rangle_b^c$ represents the rest of the terms on the right-hand side of the same equation.

Interestingly, we observe that the temporal evolution of the zero-bias current in a TS-N-TS device is controlled by the initial density of the middle N wire, the density of the Majorana bounds states formed at the inner edges of the boundary wires and the bound states of the full system. Therefore, the junction currents in Eqs. (12) and (13) can be approximated as

$$J_{\mathrm{XY}}(t) \approx 2\gamma_{\mathrm{XY}}\mathrm{Im}\left[\langle a_{2L_{\mathrm{X}}+1}^\dagger(t)a_{2L_{\mathrm{X}}-1}(t)\rangle_b^B\right], \tag{24}$$

$$J_{\mathrm{YZ}}(t) \approx 2\gamma_{\mathrm{YZ}}\mathrm{Im}\left[\langle a_{2(L_{\mathrm{X}}+L_{\mathrm{Y}})+1}^\dagger(t)a_{2(L_{\mathrm{X}}+L_{\mathrm{Y}})-1}(t)\rangle_b^B\right]. \tag{25}$$

It can be noted that the above approximation remains valid as long as the boundary wires are in the topologically nontrivial

phase away from the phase boundary. However, near the topological phase transition point, continuum states of TS wires contribute substantially to the junction currents; thus the above approximation fails. The calculated currents from such truncated computation with bound states are shown in Fig. 2 to compare them with the currents from the full simulation. They show an excellent match at long times.

Strong initial density dependence of junction currents in a TS-N-TS device can be explained with the help of Eqs. (19) and (22). For a uniform initial density $n_{l'}$ of the middle N wire, the amplitudes of the oscillating modes solely depend on the wave functions of the bounds states of the full system. Thus, the initial density of the N wire can be treated as a constant factor. However, the amplitudes of the oscillating modes are also affected by the initial densities for a nonuniform initial density at the middle wire. As the wave functions of different bound states are also spatially nonuniform, the combined effect of wave functions of bound states and inhomogeneous initial density results in suppression of the amplitudes of some selected frequency modes and (or) enhancement of others in the persistent current oscillations. So, the overall time-evolution dynamics of the density matrix for a nonuniform initial density of the middle wire behaves very differently from that for a uniform initial density.

VI. CONCLUSION

Supercurrent sensitive to initial conditions in a phase-biased superconducting nanojunction of topologically trivial BCS superconductors has been investigated in Refs. [34–37]. However, the role of initial conditions is much more intriguing and robust in the presence of midgap states or MBSs in TS wires studied here. For example, there is a persistent oscillating current even in the absence of phase-bias in a TS-N-TS device, and the amplitude of such oscillation is two orders of magnitude higher in the topologically nontrivial phase compared to the topologically trivial phase of the boundary wire. We have also shown survival of such persistent oscillating current in an experimentally realized TS system. Therefore, a detection of the zero-bias persistent oscillating current can be potentially useful as a probe of topological phase and the related topological phase transition in such hybrid devices.

It is apt to point out here some experimental challenges in detecting the zero-bias persistent current in a TS-N-TS device. There are many mechanisms including quasiparticle poisoning, stronger tunnel coupling, the presence of phonon or photon baths at the junction which can affect the lifetime of the subgap bound states exist inside the superconducting gaps. A stronger tunnel coupling between superconductors and metal or semiconductor allows for substantial single-electron tunneling from metal or semiconductor, and it is related to so-called quasiparticle poisoning. Inelastic relaxation of subgap bound states would affect the persistent current oscillation, and the zero-bias electrical current oscillation would decay with time. The TS-N-TS junction can thermalize depending on the strength of these inelastic relaxation/broadening mechanism of subgap bound states. Therefore, we suggest that experiments should be carried out at a relatively low temperature (compared to the bulk gap) with a moderate tunnel coupling (see Appendix D) and a large bulk gap for detecting the zero-bias persistent oscillating current.

The fractional Josephson effect with a characteristic 4π periodic current-phase relation in TSs has been investigated for an unambiguous detection of MZMs [5,6,19,38,39]. There are also many tunneling spectroscopy studies with N and superconducting tips to probe various magnetic and non-magnetic bound states in conventional and unconventional superconductors [10,11,40–42]. Our present dynamical study can in principle be tested in both these above setups. Our finding of lack of equilibration in the presence of bound states in a device with superconducting boundary wires having a bulk gap poses challenge for direct detection of dc or ac fractional Josephson effect as well as electrical current measurements in such device. We conclude that the necessary condition for equilibration (or a unique steady state) in these hybrid junctions is either the absence of bound states near the junctions or the band of one or both the boundary wires being continuum without a bulk gap.

ACKNOWLEDGMENTS

We are grateful to A. Dhar and D. Sen for discussions. We thank R. S. Souto for pointing Refs. [35,36] out to us. N.B. acknowledges funding from DST-FIST programme. D.R. acknowledges funding from the DST, India via the Ramanujan Fellowship.

APPENDIX A: N-TS-N DEVICE

In the main text, we have mentioned that the nonequilibrium steady-state transport in an N-TS-N device seems to be independent of the initial conditions of the finite TS wire when the band of the N wires is wider than that of the TS wire. In Fig. 5, we present plots to support our claim. In Ref. [26], the time evolution of the many-electron wave function of an N-TS junction is studied after a quantum quench in which the N and TS wires of equal and extended lengths are connected at some initial time. The decoupled N and TS wires are initially prepared in their respective ground states, and the overlap between the time-evolved wave function with the initial state (the Loschmidt echo) is found to decay with a universal power law in time for large times after the quench. We here instead prepare the decoupled N wires of our N-TS-N device initially in thermal equilibrium. In Fig. 5, we show that the electrical currents at long times do not depend on the initial density of the middle TS wire. We find from our numerics that the currents at both the junctions reach a constant nonzero value when there is a voltage bias across the TS wire due to the chemical potential difference in the boundary N wires. The simulated steady-state current in Fig. 5 from time evolution of the Heisenberg equations of motion matches with that from the Fourier transform solution at steady state [16,17].

APPENDIX B: TS-N-TS DEVICE: LONGER LENGTH OF N WIRE AND PHASE DIFFERENCE BETWEEN TS WIRES

In Fig. 6, we show how the amplitude and period of the current oscillation in a TS-N-TS device change with an increasing length of the middle N wire. The number of bound states

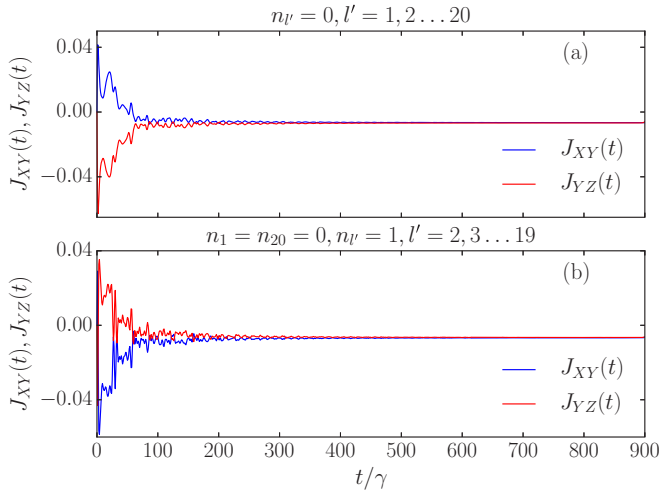

FIG. 5. Temporal evolution of the currents in an N-TS-N device under a voltage bias and presence of a unique nonequilibrium steady state. The initial density of the TS wire (modeled as a Kitaev chain) is indicated on the heading of the panels. In all panels, $L_X = L_Z = 900$, $L_Y = 20$, $\gamma_X = \gamma_Z = 1$, $\gamma_Y = 0.5$, $\Delta_X = \Delta_Z = 0$, $\Delta_Y = 0.1$, $\epsilon_X = \epsilon_Y = \epsilon_Z = 0$, $\gamma_{XY} = \gamma_{YZ} = 0.25$, $T_X = T_Z = 0.2$, and $\mu_X = -0.2$, $\mu_Z = 0.2$. All above parameters except lengths are in units of γ.

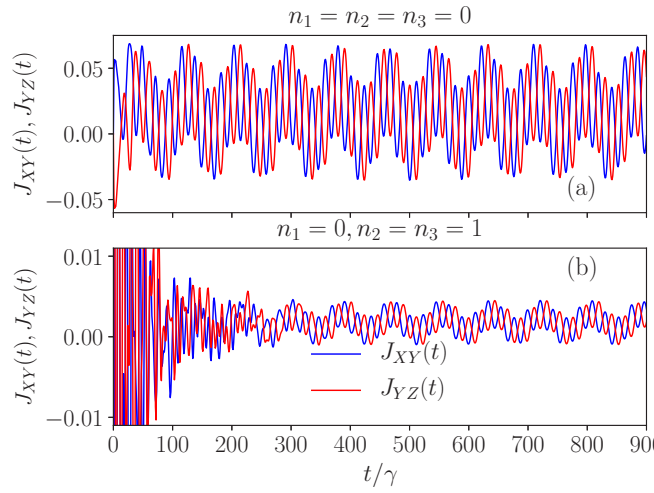

FIG. 7. Temporal evolution of the current $J_{XY}(t)$ and $J_{YZ}(t)$ in a TS-N-TS device with a phase difference of $\pi/4$ between the TS wires. The initial density of the middle N wire is indicated on the heading of the panels. In all panels, $L_X = L_Z = 900$, $L_Y = 3$, $\gamma_X = \gamma_Z = 1$, $\gamma_Y = 0.5$, $|\Delta_X| = |\Delta_Z| = 0.3$, $\phi_X = \pi/4$, $\phi_Z = 0$, $\epsilon_X = \epsilon_Z = 0$, $\epsilon_Y = 0.05$, $\gamma_{XY} = \gamma_{YZ} = 0.25$, $T_X = T_Z = 0.02$, and $\mu_X = \mu_Z = 0$. All above parameters except lengths and phases are in units of γ.

from the middle N wire can increase with increasing wire length. The current oscillations in the TS-N-TS device seem to survive for relatively long N wire length. We have seen finite persistent current oscillation in the junctions for $L_Y = 50$. However, the pattern of current oscillation, e.g., oscillation period, becomes a bit complicated in the presence of multiple bound states for a longer L_Y. We present in Fig. 6 plots for $L_Y = 4, 6$ for zero initial density of the middle N wire.

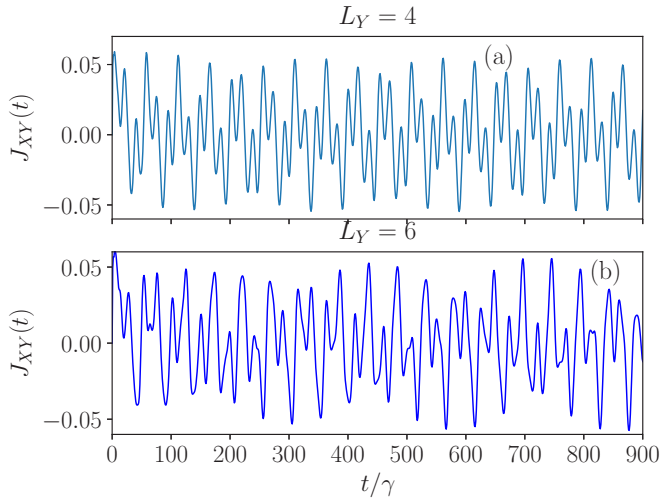

FIG. 6. Temporal evolution of the zero-bias current $J_{XY}(t)$ in a TS-N-TS for different length of the middle N wire. The length of the middle N wire is indicated on the heading of the panels. In all panels, $L_X = L_Z = 900$, $L_Y = 4, 6$, $\gamma_X = \gamma_Z = 1$, $\gamma_Y = 0.5$, $\Delta_X = \Delta_Z = 0.3$, $\epsilon_X = \epsilon_Z = 0$, $\epsilon_Y = 0.05$, $\gamma_{XY} = \gamma_{YZ} = 0.25$, $n_{l'} = 0$, and $T_X = T_Z = 0.02$. All above parameters except lengths are in units of γ.

Until now, we have discussed the dynamics in a TS-N-TS device in the absence of any phase difference between the TS wires. However, it is also interesting to study the dynamics of such a device in the presence of phase difference between the TS wires, which should in principle lead to the fractional Josephson effect. For this, we take the pairing Δ_X and Δ_Z complex, and write them as $\Delta_X = |\Delta_X| e^{i\phi_X}$ and $\Delta_Z = |\Delta_Z| e^{i\phi_Z}$. We apply a nonzero phase difference ($\phi_X - \phi_Z \neq 0$) between the TS wires modeled as the Kitaev chains. We present time evolution of electrical current at the left and right junctions of the TS-N-TS device in Figs. 7 and 8 in the absence of any thermal or voltage bias. Similar to Fig. 2, we

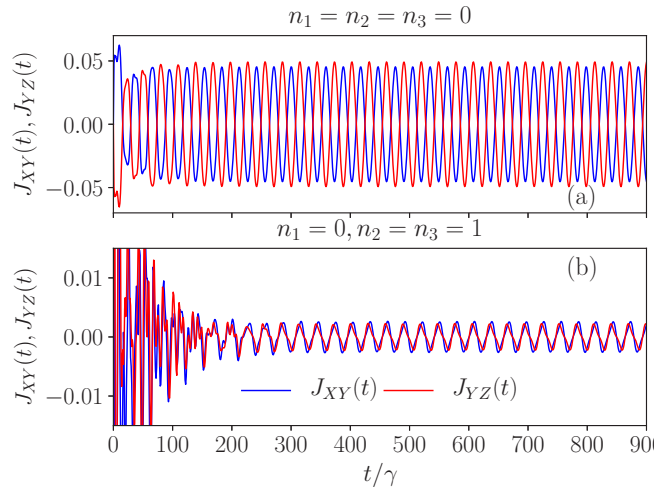

FIG. 8. Temporal evolution of the current $J_{XY}(t)$ and $J_{YZ}(t)$ in a TS-N-TS device with a phase difference of π between the TS wires. All the parameters except $\phi_X = \pi$ are as in Fig. 7.

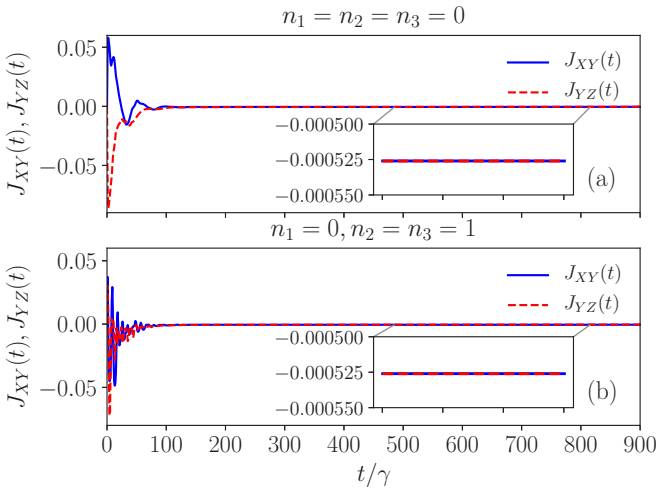

FIG. 9. Temporal evolution of the currents in a TS-N-N device under a voltage bias and presence of a unique nonequilibrium steady state. The initial density of the middle N wire is indicated on the heading of the panels. In all panels, $L_X = L_Z = 900$, $L_Y = 3$, $\gamma_X = \gamma_Z = 1$, $\gamma_Y = 0.5$, $\Delta_X = 0.2$, $\Delta_Y = \Delta_Z = 0$, $\epsilon_X = 0.02$, $\epsilon_Y = 0.05$, $\epsilon_Z = 0$, $\gamma_{XY} = \gamma_{YZ} = 0.25$, $T_X = T_Z = 0.2$, and $\mu_X = 0$, $\mu_Z = 0.5$. All above parameters except lengths are in units of γ.

again find the current at the junctions depends on the initial conditions of the middle wire indicating the absence of unique steady state.

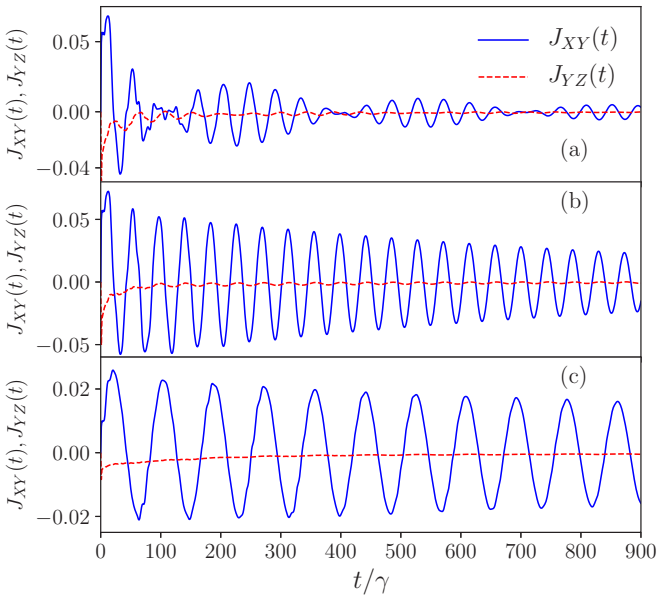

FIG. 10. Temporal evolution of the currents in a TS-N-Z device when the on-site energy of the superconducting Z wire is swept through the topological phase transition, and role of tunnel coupling. The blue full lines are for $J_{XY}(t)$ and the red dashed lines are for $J_{YZ}(t)$. The on-site energy $\epsilon_Z = 1.99, 2.05, 2.05$ and tunnel coupling $\gamma_{YZ} = 0.25, 0.25, 0.1$ in panels (a)–(c), respectively. In all panels, $L_X = L_Z = 900$, $L_Y = 3$, $\gamma_X = \gamma_Z = 1$, $\gamma_Y = 0.5$, $\Delta_X = \Delta_Z = 0.3$, $\epsilon_X = 0$, $\epsilon_Y = 0.05$, $\gamma_{XY} = 0.25$, $n_{l'} = 0$, and $T_X = T_Z = 0.02$. The above parameters (except lengths) are in units of γ.

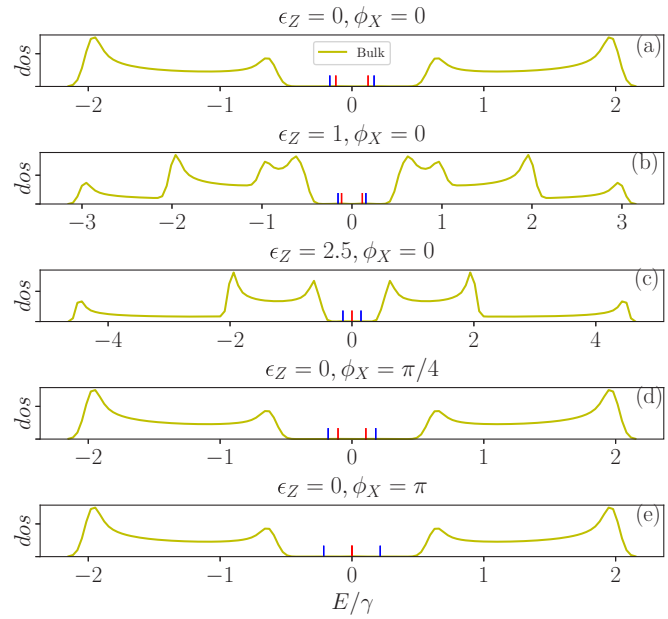

FIG. 11. Density of energy eigenstates (*dos*) of a TS-N-Z device with different on-site energy of the superconducting Z wire and various phase difference between the boundary wires. The red and blue lines (arbitrary scale) denote the energy eigenvalues of midgap states near the junction originating from the boundary TS wires and the middle N wire, respectively. The on-site energy $\epsilon_Z = 0, 1, 2.5, 0, 0$ and the phase $\phi_X = 0, 0, 0, \pi/4, \pi$ in panels (a)–(e), respectively. In all panels, $L_X = L_Z = 900$, $L_Y = 3$, $\gamma_X = \gamma_Z = 1$, $\gamma_Y = 0.5$, $\Delta_X = \Delta_Z = 0.3$, $\epsilon_X = 0$, $\epsilon_Y = 0.05$, $\gamma_{XY} = \gamma_{YZ} = 0.25$, and $\phi_Z = 0$. The above parameters (except lengths) are in units of γ.

Nevertheless, in contrast to zero time-averaged currents in the absence of phase-bias in Figs. 2 and 3, the time-averaged currents in Fig. 7 are nonzero when $\phi_X - \phi_Z = \pi/4$, although the time-averaged currents in Fig. 8 are again zero when $\phi_X - \phi_Z = \pi$. The time-averaged current seems to have a 2π periodicity over the phase difference instead of a 4π periodicity for the dc fractional Josephson effect in a phase-biased Josephson junction. Similar initial-condition-dependent Josephson current and related quasiparticle trapping in superconducting point contacts of topologically trivial *s*-wave superconductors have been studied in recent years [34–36].

APPENDIX C: TS-N-N DEVICE

We have gotten a unique nonequilibrium steady state in a TS-N-N device, and we do not see here any persistent electrical current oscillation in the absence of voltage or temperature bias. In Fig. 9, we plot electrical currents at both the junctions of a TS-N-N device for two different initial densities in the middle N wire. We also apply a voltage bias across the middle N wire by using a nonzero chemical potential for the boundary N wire. We find that the electrical currents at both junctions are independent of the initial density in the middle N wire. The nonequilibrium steady-state currents are also the same at both intersections. Therefore, we conclude that the middle N wire in a TS-N-N device equilibrates with the boundary wires due to a continuous band of the boundary N wire.

APPENDIX D: ROLE OF TUNNEL COUPLING

In the main text, we have discussed equilibration in a TS-N-Z device when the Z wire transits through a topological phase transition. The closing of superconducting bulk gap near the topological phase transition is the reason for equilibration. In Fig. 10, we further show that the electrical current in a TS-N-Z device decays to zero at long times when there is a bulk gap in the Z wire which is the smaller or same order of γ_{YZ}^2. The tunnel coupling γ_{YZ} induces broadening of the energy of the bound states. Thus, the energy-broadened bound states near the junctions can overlap with the band (delocalized states) of the Z wire when the bulk-gap is small. Therefore, we expect equilibration of bound states and decay of electrical currents when the ratio between the bulk gap and γ_{YZ}^2 is low. For example, this ratio is 0.16, 0.8, 5, respectively, for three plots in Figs. 10(a)–10(c). While the current $J_{XY}(t)$ in Figs. 10(a) and 10(b) shows clear decay with time, the decay of $J_{XY}(t)$ is relatively slow in Fig. 10(c). Therefore, a stronger tunnel coupling can effectively reduce the bulkgap in superconducting boundary wires and hence can help in equilibration. Nevertheless, there can also be other mechanisms of equilibration such as electron-phonon interaction at the middle wire or irradiation of radiation on the Josephson junctions for the measurement of Shapiro steps in current-voltage curves. The bound states can equilibrate when the phonon or the radiation at the junctions is wide band such that the band of phonon or radiation closes the superconducting gaps.

APPENDIX E: ENERGY SPECTRA OF THE TS-N-TS DEVICE

The properties (especially the periods) of persistent current oscillations in the TS-N-TS device depend on the energy eigenvalues of the midgap states originating from the boundary TS wires as well as the middle N wire. In Fig. 11, we present some examples of these energy eigenvalues along with the density of energy eigenstates (*dos*) of the bulk spectrum of the full TS-N-Z device. We particularly select those values of on-site energy of the superconducting Z wire and phase difference between the boundary wires which are used in Figs. 2, 3(a), 3(c), 7, and 8. The energy of the MBSs is almost zero in the absence of hybridization through the middle wire when the phase difference between the boundary TS wires is π, or one of the boundary superconducting wires is nontopological. While the periods of persistent current oscillations are sensitive to the energy of midgap states, the amplitude of the persistent current oscillations is large as long as there is a midgap state at that junction from the adjoining boundary TS wire.

[1] J. Alicea, Rep. Prog. Phys. **75**, 076501 (2012).
[2] C. Beenakker, Annu. Rev. Condens. Matter Phys. **4**, 113 (2013).
[3] T. D. Stanescu and S. Tewari, J. Phys. Condens. Matter **25**, 233201 (2013).
[4] S. R. Elliott and M. Franz, Rev. Mod. Phys. **87**, 137 (2015).
[5] A. Y. Kitaev, Phys. Usp. **44**, 131 (2001).
[6] R. M. Lutchyn, J. D. Sau, and S. Das Sarma, Phys. Rev. Lett. **105**, 077001 (2010).
[7] Y. Oreg, G. Refael, and F. von Oppen, Phys. Rev. Lett. **105**, 177002 (2010).
[8] V. Mourik, K. Zuo, S. M. Frolov, S. R. Plissard, E. P. A. M. Bakkers, and L. P. Kouwenhoven, Science **336**, 1003 (2012).
[9] A. Das, Y. Ronen, Y. Most, Y. Oreg, M. Heiblum, and H. Shtrikman, Nat. Phys. **8**, 887 (2012).
[10] S. Nadj-Perge, I. K. Drozdov, J. Li, H. Chen, S. Jeon, J. Seo, A. H. MacDonald, B. A. Bernevig, and A. Yazdani, Science **346**, 602 (2014).
[11] M. Ruby, F. Pientka, Y. Peng, F. von Oppen, B. W. Heinrich, and K. J. Franke, Phys. Rev. Lett. **115**, 197204 (2015).
[12] S. M. Albrecht, A. P. Higginbotham, M. Madsen, F. Kuemmeth, T. S. Jespersen, J. Nygard, P. Krogstrup, and C. M. Marcus, Nature **531**, 206 (2016).
[13] C. J. Bolech and E. Demler, Phys. Rev. Lett. **98**, 237002 (2007).
[14] K. T. Law, P. A. Lee, and T. K. Ng, Phys. Rev. Lett. **103**, 237001 (2009).
[15] K. Flensberg, Phys. Rev. B **82**, 180516(R) (2010).
[16] D. Roy, C. J. Bolech, and N. Shah, Phys. Rev. B **86**, 094503 (2012).
[17] D. Roy, N. Bondyopadhaya, and S. Tewari, Phys. Rev. B **88**, 020502(R) (2013).
[18] A. Zazunov, R. Egger, and A. Levy Yeyati, Phys. Rev. B **94**, 014502 (2016).
[19] L. P. Rokhinson, X. Liu, and J. K. Furdyna, Nat. Phys. **8**, 795 (2012).
[20] A. Zazunov and R. Egger, Phys. Rev. B **85**, 104514 (2012).
[21] P. San-Jose, J. Cayao, E. Prada, and R. Aguado, New J. Phys. **15**, 075019 (2013).
[22] P. A. Ioselevich, P. M. Ostrovsky, and M. V. Feigel'man, Phys. Rev. B **93**, 125435 (2016).
[23] J. Cayao, P. San-Jose, A. M. Black-Schaffer, R. Aguado, and E. Prada, Phys. Rev. B **96**, 205425 (2017).
[24] Y. Peng, F. Pientka, Y. Vinkler-Aviv, L. I. Glazman, and F. von Oppen, Phys. Rev. Lett. **115**, 266804 (2015).
[25] G. Sharma and S. Tewari, Phys. Rev. B **93**, 195161 (2016).
[26] R. Vasseur, J. P. Dahlhaus, and J. E. Moore, Phys. Rev. X **4**, 041007 (2014).
[27] S. Hegde, V. Shivamoggi, S. Vishveshwara, and D. Sen, New J. Phys. **17**, 053036 (2015).
[28] P. D. Sacramento, Phys. Rev. E **93**, 062117 (2016).
[29] D. Dahan, M. T. Ahari, G. Ortiz, B. Seradjeh, and E. Grosfeld, Phys. Rev. B **95**, 201114(R) (2017).
[30] A. Dhar and D. Sen, Phys. Rev. B **73**, 085119 (2006).
[31] J.-P. Blaizot and G. Ripka, *Quantum Theory of Finite Systems* (MIT Press, Cambridge, MA, 1986).
[32] D. Rossini, T. Calarco, V. Giovannetti, S. Montangero, and R. Fazio, Phys. Rev. A **75**, 032333 (2007).
[33] An N-TS junction is only considered in many of these studies.

[34] M. Zgirski, L. Bretheau, Q. Le Masne, H. Pothier, D. Esteve, and C. Urbina, Phys. Rev. Lett. **106**, 257003 (2011).
[35] R. S. Souto, A. Martín-Rodero, and A. L. Yeyati, Phys. Rev. Lett. **117**, 267701 (2016).
[36] R. S. Souto, A. Martín-Rodero, and A. L. Yeyati, Phys. Rev. B **96**, 165444 (2017).
[37] R. Taranko, T. Kwapinski, and T. Domanski, Phys. Rev. B **99**, 165419 (2019).
[38] H.-J. Kwon, K. Sengupta, and V. M. Yakovenko, Eur. Phys. J. B **37**, 349 (2004).
[39] C. Li, J. C. de Boer, B. de Ronde, S. V. Ramankutty, E. van Heumen, Y. Huang, A. de Visser, A. A. Golubov, M. S. Golden, and A. Brinkman, Nat. Mater. **17**, 875 (2018).
[40] A. Yazdani, C. M. Howald, C. P. Lutz, A. Kapitulnik, and D. M. Eigler, Phys. Rev. Lett. **83**, 176 (1999).
[41] E. W. Hudson, K. M. Lang, V. Madhavan, S. H. Pan, H. Eisaki, S. Uchida, and J. C. Davis, Nature **411**, 920 (2001).
[42] S.-H. Ji, T. Zhang, Y.-S. Fu, X. Chen, X.-C. Ma, J. Li, W.-H. Duan, J.-F. Jia, and Q.-K. Xue, Phys. Rev. Lett. **100**, 226801 (2008).